JACS
JOURNAL OF THE AMERICAN CHEMICAL SOCIETY
pubs.acs.org/JACS
Article

Giant Concentric Metallosupramolecule with Aggregation-Induced Phosphorescent Emission

Yiming Li,[‖] Gui-Fei Huo,[‖] Bingqing Liu, Bo Song, Yuan Zhang, Xiaomin Qian, Heng Wang, Guang-Qiang Yin, Alexander Filosa, Wenfang Sun, Saw Wai Hla, Hai-Bo Yang, and Xiaopeng Li*

Cite This: https://dx.doi.org/10.1021/jacs.0c06680

Read Online

ACCESS | Metrics & More | Article Recommendations | Supporting Information

ABSTRACT: Fluorescent metallosupramolecules have received considerable attention due to their precisely controlled dimensions as well as the tunable photophysical and photochemical properties. However, phosphorescent analogues are still rare and limited to small structures with low-temperature phosphorescence. Herein, we report the self-assembly and photophysical studies of a giant, discrete metallosupramolecular concentric hexagon functionalized with six alkynylplatinum(II) bzimpy moieties. With a size larger than 10 nm and molecular weight higher than 26 000 Da, the assembled terpyridine-based supramolecule displayed phosphorescent emission at room temperature. Moreover, the supramolecule exhibited enhanced aggregation-induced phosphorescent emission compared to the ligand by tuning the aggregation states through intermolecular interactions and significant enhancement of emission to CO_2 gas.

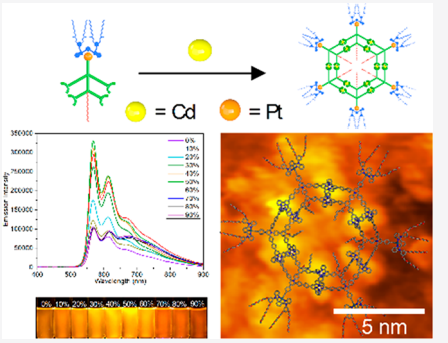

INTRODUCTION

Discrete metallosupramolecules obtained via coordination-driven self-assembly have emerged as a class of materials to bridge the gap between small molecules and polymers[1] on account of the precisely controlled dimensions that provide an ideal platform for investigations of structure−property−function relationships.[2] Among the various functions, the luminescence of metallosupramolecules has a wide range of applications in sensing,[3] photocatalysis,[4] bioimaging,[5] light harvesting,[6] phototherapy[7] and so on.[8] Emissive metallosupramolecules have been constructed mainly through the following three strategies: (i) introducing the luminophores into the scaffolds;[9] (ii) attaching the luminophores on the backbone as accessories;[7c,10] and (iii) encapsulating luminophores in the cavity of the structures through host−guest chemistry.[8f,11] Generally, the luminophores include small organic motifs, such as tetraphenylethylene,[12] boron-dipyrromethene (BODIPY),[5b,13] triphenylamine,[14] pyrene,[15] and perylene diimide,[16] as well as emissive metal complexes containing Ru(II),[17] Eu(III),[18] Ir(III),[6a,10,19] Pt(II),[20] and Au(I).[21] Among these emissive metallosupramolecules, however, phosphorescent analogues are still rare and mainly limited to small structures with low-temperature phosphorescence.[18d,20a,21a,22]

2,2′:6′,2′′-Terpyridine (tpy), as one of the most intensively investigated building blocks, has been widely used in constructing sophisticated metallosupramolecular architectures with well-defined sizes, shapes, and geometries.[23] With weak luminescence, tpy has been functionalized with many luminophores to tune the emissive properties of corresponding metal complexes.[24] For instance, Cd(II) was frequently assembled with tpy to construct fluorescent supramolecules,[25] among which characteristic aggregation-induced emission (AIE)[12a,26] was observed. Recent examples further employed tpy building blocks to construct phosphorescent metallopolymers.[27] Among the luminophores, square-planar Pt(II) motifs have received considerable attention because of their unique photophysical and electrochemical properties.[28] These complexes exhibit phosphorescence brought by the heavy-atom effect with tunable emission wavelengths and lifetimes.[28b,29] Also, Pt(II) luminophores are prone to have strong intermolecular Pt···Pt interaction,[30] which can manipulate their aggregations and enable emission through the aggregation-induced phosphorescent emission (AIPE) effect,[31] a variant of AIE. More importantly, Pt(II) complexes are thermodynamically stable and kinetically inert.[28a] Thus, such features facilitate the synthesis of tpy building blocks with Pt(II) luminophores for further coordination-driven self-assembly.

On the basis of a previous study, we speculated the combination of AIPE-active Pt(II) components with tpy-based emissive supramolecules could create a synergy by which the emissive properties of individual components could be retained

Received: June 21, 2020

Downloaded via TRINITY COLG DUBLIN on August 15, 2020 at 03:01:17 (UTC).
See https://pubs.acs.org/sharingguidelines for options on how to legitimately share published articles.

© XXXX American Chemical Society

Scheme 1. Synthesis of Ligand L and Self-Assembly of Metallosupramolecule S

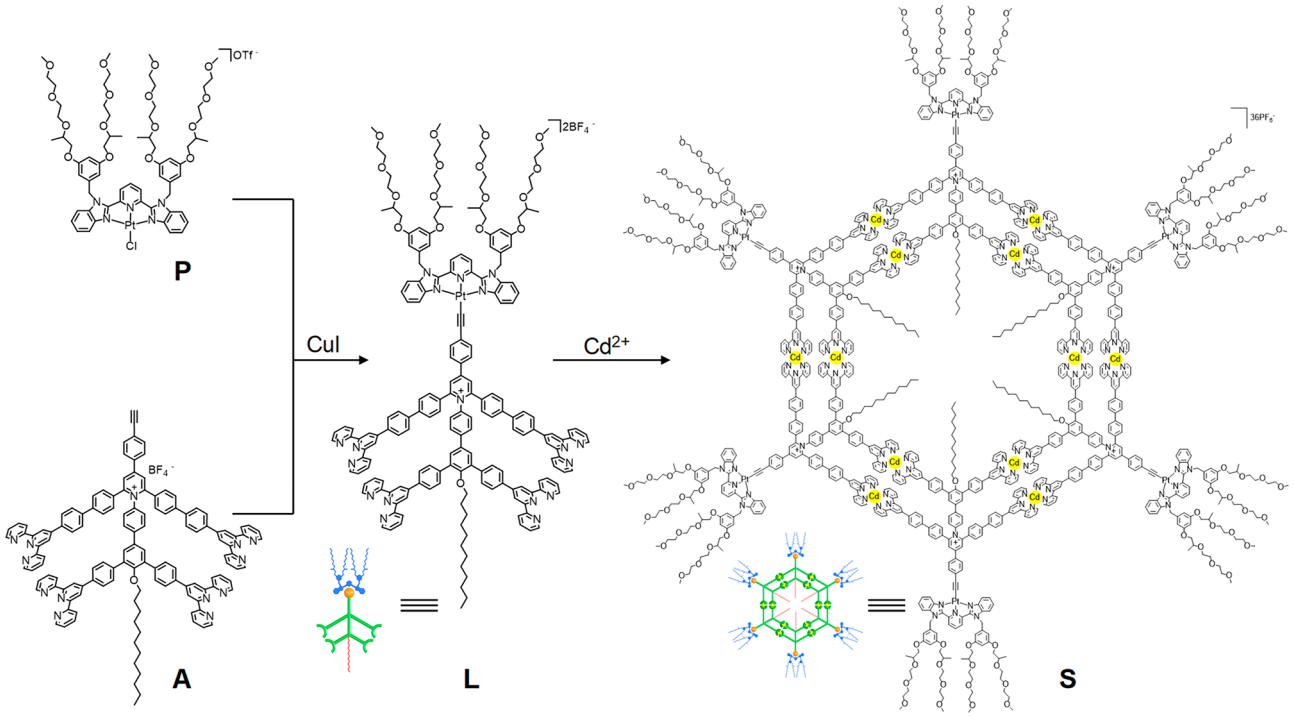

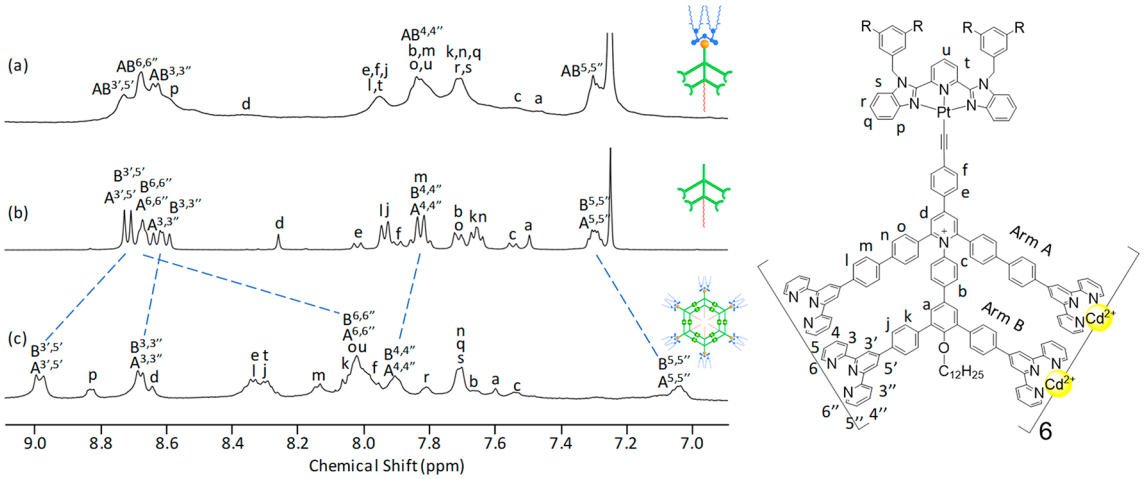

Figure 1. ^{1}H NMR spectra of (a) **L** in $CDCl_3$, (b) **A** in $CDCl_3$, and (c) **S** in CD_3CN. Broad signals of **L** were attributed to the strong aggregation in solution.

and the hybrid supramolecular architectures could even display superior AIPE compared to the individual components. According to this speculation, we designed a giant but discrete metallosupramolecular concentric hexagon (**S**) functionalized with six Pt(II) bzimpy (bzimpy = 2,6-bis(benzimidazole-2′-yl) pyridine) motifs. In the design, a terminal alkynyl group was employed to install the Pt(II) motif with a stable and rigid Pt(II)−alkynyl bond for further self-assembly. Also, we introduced multiple hydrophilic ethylene glycol chains into bzimpy moieties on the periphery and a long alkyl chain (C12) into the interior to tune the aggregation through balancing the overall hydrophobicity/hydrophilicity. With a size larger than 10 nm and a molecular weight higher than 26 000 Da, the assembled tpy-based supramolecule containing six Pt(II) centers displayed phosphorescent emission with a lifetime of 218 ns at room temperature. By synergistically combining AIPE from Pt(II) luminophores and AIE features from Cd(II)−tpy assemblies, the functionalized supramolecule **S** exhibited significantly enhanced AIPE compared to the ligand **L**. Via tuning the aggregation states of the functionalized ligand **L** and **S**, their AIPE behaviors were carefully investigated. More interestingly, further enhancement of phosphorescent emission was observed in both **L** and **S** when purged by CO_2 gas. As such, this system is expected to find practical applications, such as gas sensing.

RESULTS AND DISCUSSION

In the synthesis of building block **L**, Scheme 1, tetratopic tpy-pyridinium salt precursor **A** was synthesized using a modified procedure as previously reported.[23h] A terminal alkynyl group was introduced into the backbone of **A** in order to further functionalize the metallosupramolecule, including installation

https://dx.doi.org/10.1021/jacs.0c06680
J. Am. Chem. Soc. XXXX, XXX, XXX−XXX

of the following Pt(II) motif with the stable and rigid Pt(II)−alkynyl bond. The detailed synthesis procedures for **A** (Scheme S2) and chloroplatinum(II) bzimpy precursor **P** (Scheme S3) are described in the Supporting Information (SI). The final alkynylplatinum(II) bzimpy ligand **L** was synthesized by bridging **P** and **A** in the presence of a catalytic amount of copper(I) iodide and triethylamine in DMF solution under N_2 atmosphere.

All of the ligands and precursors were fully characterized by multidimensional nuclear magnetic resonance (NMR), including ^{1}H, ^{13}C, 2D correlation spectroscopy (2D COSY), and/or nuclear Overhauser effect spectroscopy (NOESY), as well as electrospray ionization mass spectrometry (ESI-MS) (see details in SI). It is noteworthy that the proton resonance of ligand **L** showed very broad signals in $CDCl_3$ (Figure 1a), as well as in CD_3CN (Figure S38). In contrast, the proton resonance for the Pt(II) free precursor **A** displayed sharp signals (Figure 1b). All of these results suggested that **L** was highly prone to aggregate in solutions through intermolecular Pt···Pt and $\pi-\pi$ interactions.[32]

The self-assembly of **S** was achieved by treating **L** with $Cd(NO_3)_2$ in a stoichiometric ratio of 1:2, followed by counterion exchange with excess NH_4PF_6 to give **S** as a yellow precipitate in a high yield. The ^{1}H NMR spectrum of the supramolecule (Figure 1c) showed much sharper signals compared with the spectrum of **L**, indicating weaker aggregation of **S** owing to the bulky size of the octahedral coordination of the ⟨tpy−Cd(II)−tpy⟩ unit that reduced the intermolecular Pt···Pt interactions. Two characteristic singlets with an integration ratio of 1:1 were observed at 9.00 and 8.97 ppm, respectively, which were assigned to the tpy-$H^{3',5'}$ protons of the inner and outer layer, excluding formation of polymeric species. Compared with those of **A**, the tpy-$H^{3',5'}$ signals of **S** showed a diagnostic downfield shift (ca. 0.3 ppm) while the tpy-$H^{6,6''}$ peaks exhibited a significantly upfield shift (ca. 0.7 ppm), indicating complexation of tpy units with Cd(II). Diffusion ordered spectroscopy (DOSY) NMR of **S** revealed a narrow band with diffusion coefficient log D = −9.20 at 298 K (Figure S50), suggesting formation of a discrete structure. All of the assignments were further supported by 2D COSY and NOESY spectra (Figures S45−S49).

In addition, electrospray ionization-mass spectrometry (ESI-MS) and traveling wave ion mobility-mass spectrometry (TWIM-MS)[33] were used to characterize the functionalized supramolecule. A series of peaks with continuous charges from 13+ to 24+ was observed in ESI-MS (Figure 2a) due to the successive loss of PF_6^- counterions. After deconvolution, the molecular weight was calculated as 26 301 Da, corresponding to the chemical composition of $C_{1188}H_{1152}N_{108}O_{102}Pt_6Cd_{12}P_{36}F_{216}$. The experimental isotope pattern of each charge state agreed well with the corresponding simulated peak (Figure 2a inset, Figure S63). Moreover, only one set of signals was observed from TWIM-MS, indicating that there was no other structural conformer or isomer for the assembled structure (Figure 2b).

To further study the structure of the supramolecule, transmission electron microscopy (TEM) was utilized to verify the size and shape of **S**. The supramolecules were observed as a dispersion of individual uniform dots (Figure 3b). The average size of the particles was in good agreement with the theoretical diameter calculated by molecular modeling (Figure 3a and 3c). In order to directly visualize the structure

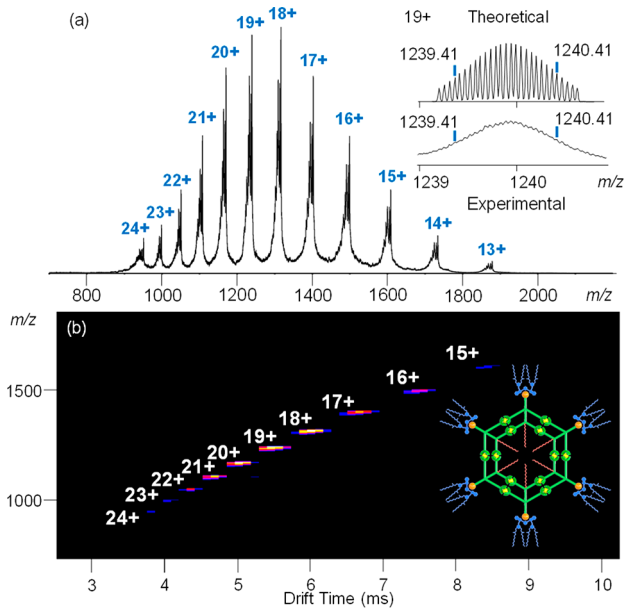

Figure 2. (a) ESI-MS and (b) TWIM-MS plots of **S**.

of the metallosupramolecules with high resolution, ultrahigh-vacuum-low-temperature-scanning tunneling microscopy (UHV-LT-STM) was also applied.[23k,34] Ultrahigh vacuum provided a clean and neat environment to minimize noise, and low temperature would reduce thermal motion, thus leading to a higher resolution. A very dilute solution of **S** was drop casted on a Ag(111) substrate followed by cooling down to 4 K. Due to the octahedral coordination and high electron density around the metal center, the STM imaging showed six elliptic bright dots corresponding to ⟨tpy−Cd(II)−tpy⟩ units, which depicted the framework of a hexagonal structure (Figure 3d−f). Within the magnified image, the shape and direction of each elliptic-shaped lobe can be distinctly observed. Note that each dot was attributed to the fusion of signals from two ⟨tpy−Cd(II)−tpy⟩ units in the two layers because of the short distance between them. Moreover, the double-layered scaffold without Pt(II) motifs was measured to have a diameter of ∼8 nm and a height of ∼10 Å (Figure 3f−h), which agreed well with the theoretical modeling (Figure 3a). In sharp contrast to the bright lobes of ⟨tpy−Cd(II)−tpy⟩ units in STM measurement, Pt atoms did not exhibit strong signals. We speculated that the bulky ⟨tpy−Cd(II)−tpy⟩ unit with octahedral coordination geometry might lift the entire organic moieties off the substrate, as well as the end groups of alkynyl−Pt bzimpy. Therefore, the square-planar Pt(II) center could have less contact with the surface, leading to the loss of tunneling current.

After the structural characterization, the emission properties of **S**, **L**, and the precursors **A** and **P** were investigated in acetonitrile solutions (mixed with 5% CH_2Cl_2 for **A**) at room temperature. The normalized emission spectra are shown in Figure 4a, and the emission parameters, including emission wavelengths and lifetimes, are listed in Table S1. The emissions of **P**, **L**, and **S** exhibited large Stokes shifts (>200 nm) with respect to their corresponding absorption bands (Figure S64)[35] and were prone to oxygen quenching. In addition, the recorded emission lifetimes of **L** and **S** deduced from the decay traces were 270 and 218 ns, respectively (Figure 4b and 4c), which are longer than those of general

https://dx.doi.org/10.1021/jacs.0c06680
J. Am. Chem. Soc. XXXX, XXX, XXX−XXX

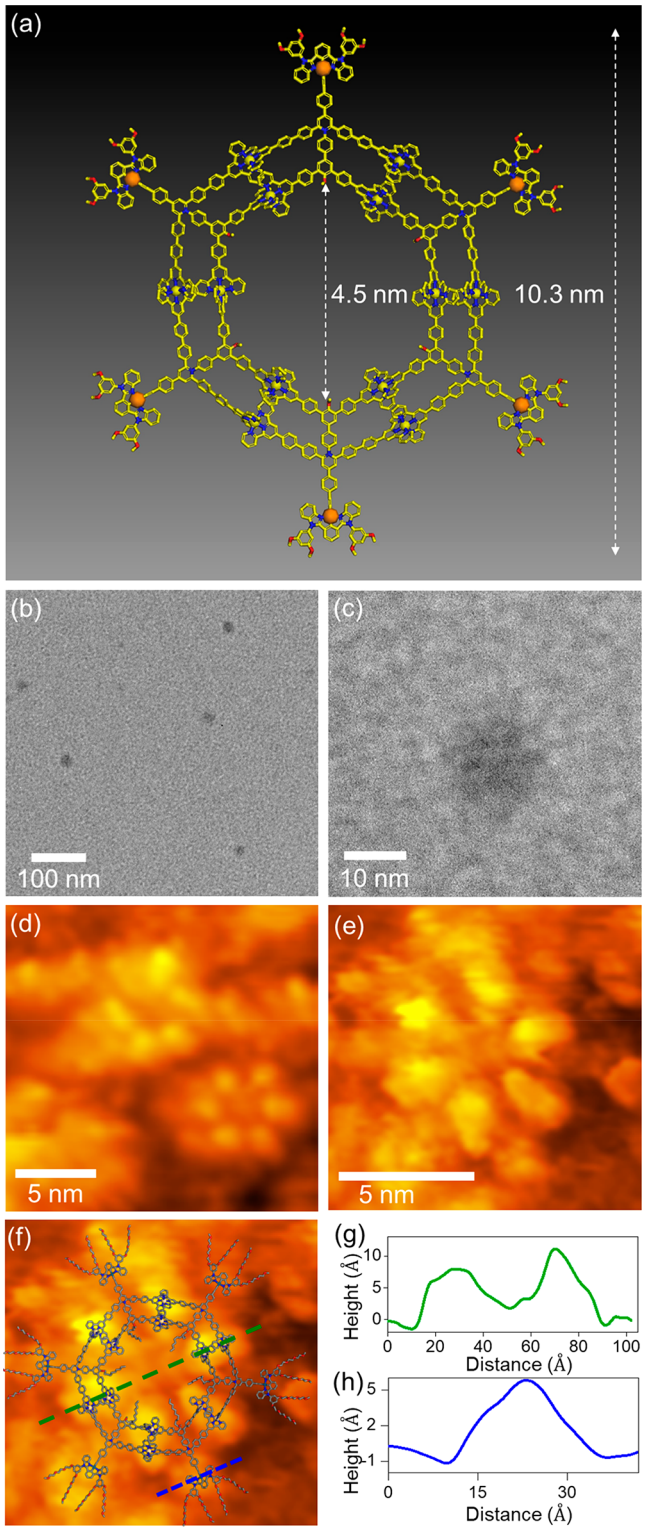

Figure 3. TEM and STM imaging of **S**. (a) Molecular modeling of **S** (ethylene glycol and alkyl chains were omitted for clarity). (b) TEM image of **S**. (c) Magnified TEM image of **S**. (d) Large area STM image of **S** showing the presence of two supramolecules (imaging parameters: V_t = 2.5 V and I_t = 35 pA). (e) Magnified image of a single supramolecule. (f) STM image of **S** with molecular modeling overlay (imaging parameters: V_t = 2.5 V and I_t = 29 pA). (g and h) STM line profiling measurements were performed along the green and blue dashed lines shown in f.

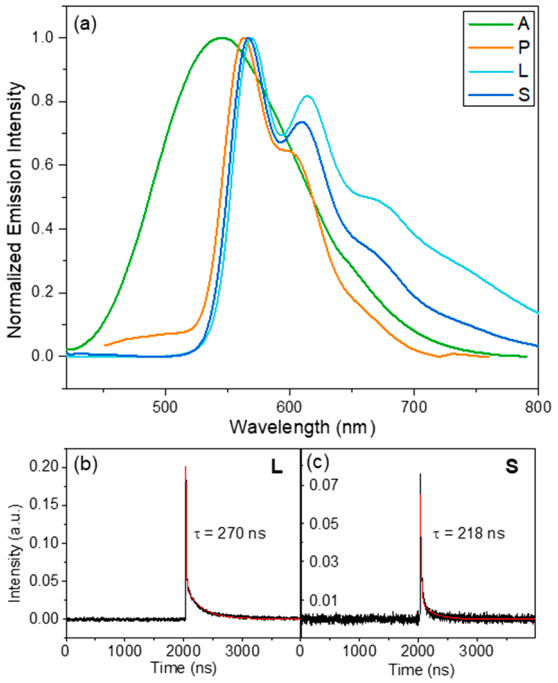

Figure 4. (a) Normalized emission spectra of **P** and **A** (λ_{ex} = 390 nm) and **L** and **S** (λ_{ex} = 370 nm) in N_2 deoxygenated acetonitrile (with 5% CH_2Cl_2 for **A**) at room temperature ($c = 1 \times 10^{-5}$ mol/L). Emission lifetime decay traces of (b) **L** and (c) **S**.

fluorescence. These features implied a nature of room-temperature phosphorescence through the emission from the triplet excited states.

The emission spectra of **P**, **L**, and **S** resembled each other with essentially the same energy and similar vibronic progressions, indicating the same/similar original emitting excited states. The vibronic spacing between the band maxima (ca. 567 nm) and the shoulder (ca. 606 nm) was approximately 1135 cm^{-1}, which is in accordance with the stretching mode of the aromatic rings.[35] Also, broad tails were observed in **L** and **S** compared to **P** due to the metal-metal-to-ligand charge transfer(^{3}MMLCT) excited states from the Pt···Pt and $\pi-\pi$ stacking interactions.[32] In view of the similar structural component in these three complexes, i.e., bzimpy, a similar $[(N^N^N)PtCl]^+$ complex was reported in the literature, we attribute the observed emission originating from the metal-perturbed $^3\pi,\pi^*$ emission of the bzimpy.[36] Pt(II)-contained precursor **P** exhibited short-lived emission of 18 ns (Figure S65). This phenomenon could be ascribed to the presence of a thermally accessible low-lying metal-centered nonemissive ^{3}d,d state, which provided an additional decay pathway and quenched the ligand-localized $^3\pi,\pi^*$ emission. This is a common feature in many other $[(N^N^N)PtCl]^+$ complexes.[37] When the Cl ligand in **P** was replaced by the acetylide ligand in **L**, the electron-donating ability of the acetylide ligand lifted up the ^{3}d,d state with a negligible impact on the energy of the $^3\pi,\pi^*$ state. This separated the nonemissive ^{3}d,d state from the emitting $^3\pi,\pi^*$ state further and consequently improved the emission in **L**. Introduction of heavy-atom Cd(II) during the self-assembly of **L** into **S** could induce intersystem crossing (a competing nonradiative thermal process with the radiative decay path) from T_1 to S_0. Meanwhile, the weak ligand field strength of the Cd(II) ion would narrow the energy gap between the nonemissive ^{3}d,d

https://dx.doi.org/10.1021/jacs.0c06680
J. Am. Chem. Soc. XXXX, XXX, XXX−XXX

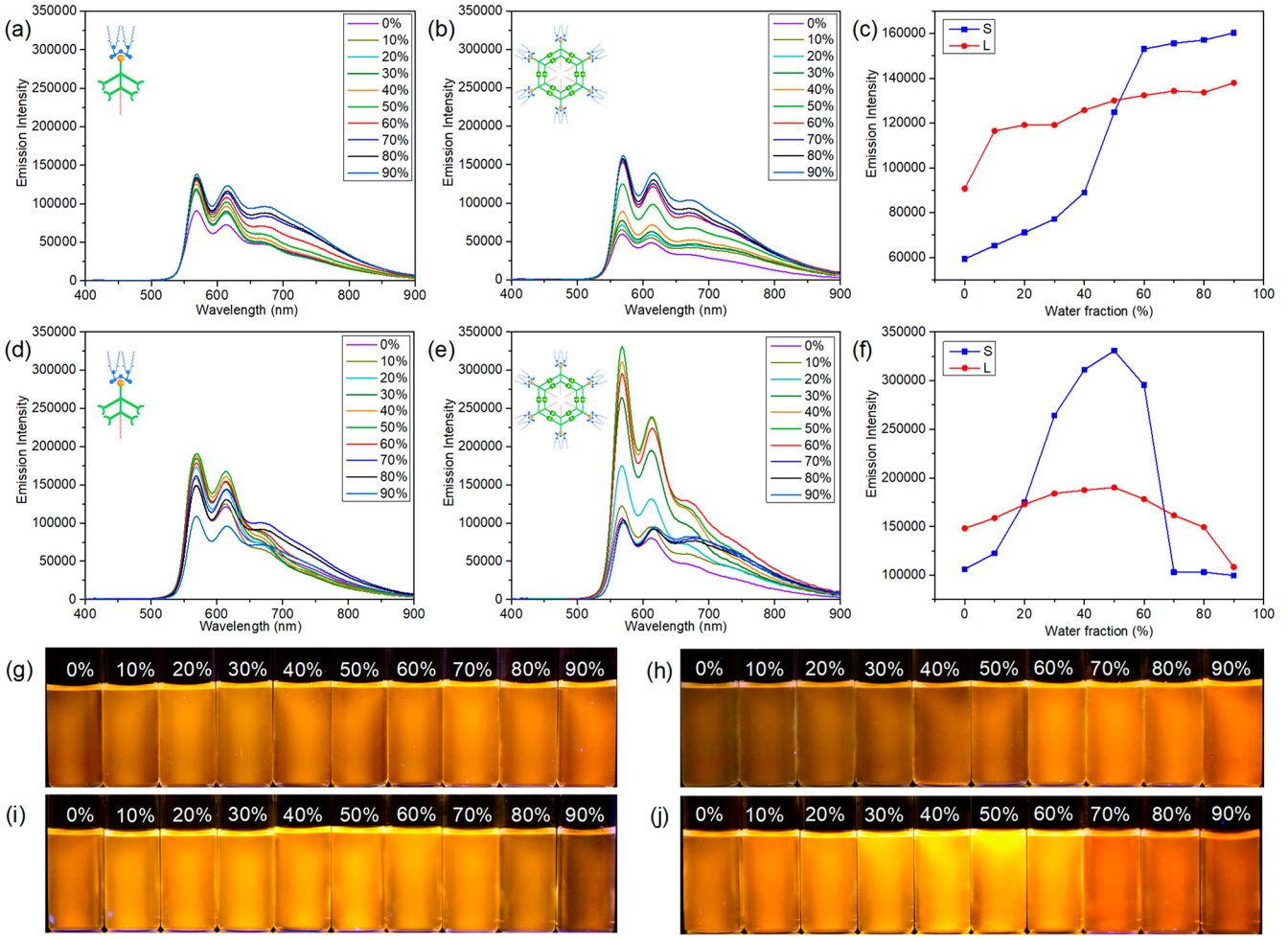

Figure 5. Emission spectra of **L** and **S**. (a) Emission spectra of ligand **L** in nondeoxygenated acetonitrile/water solvent (λ_{ex} = 370 nm, c = 3.5 μM). (b) Emission spectra of **S** in nondeoxygenated acetonitrile/water solvent (λ_{ex} = 370 nm, c = 0.6 μM). (c) Emission intensity of **L** and **S** at 567 nm with different fractions of water in nondeoxygenated acetonitrile/water solution. (d) Phosphorescent emission spectra of **L** with N_2 deoxygenated acetonitrile/water solvent (λ_{ex} = 370 nm, c = 3.5 μM). (e) Phosphorescent emission spectra of **S** with N_2 deoxygenated acetonitrile/water solvent (λ_{ex} = 370 nm, c = 0.6 μM). (f) Emission intensity of **L** and **S** at 567 nm with different fractions of water in N_2 deoxygenated acetonitrile/water solution. (g) Emission photographs of **L** in nondeoxygenated acetonitrile/water with various water fractions. (h) Emission photographs of **S** in nondeoxygenated acetonitrile/water with various water fractions. (i) Emission photographs of **L** in N_2 deoxygenated acetonitrile/water with various water fractions (under 365 nm UV lamp). (j) Emission photographs of **S** in N_2 deoxygenated acetonitrile/water with various water fractions (under 365 nm UV lamp).

state and the emitting $^3\pi,\pi^*$ state, which would decrease the lifetime of **S**. Interestingly, **S** still retained a relatively long lifetime of 218 ns. It is worth noting that these phosphorescent properties are quite unique for such a giant supramolecule with a diameter of 10 nm.

To investigate the intermolecular interactions within ligands and supramolecules, temperature-dependent emission studies were performed (Figure S66). The spectra of both **L** and **S** showed that with the elevation of the temperature, the intensity of the emission decreased dramatically as the noncovalent interactions could become negligible at high temperature.[38] These results suggested the existence of Pt···Pt interactions in both ligand **L** and supramolecule **S** at room temperature. Indeed, formation of aggregations by Pt···Pt interactions brought the restriction of an intramolecular rotation (RIR) effect at low temperature[26d,e] and immobilized the luminophores on the molecules, leading to the enhancement of emission.

Further detailed photophysical studies of **L** and **S** were performed in acetonitrile/water mixed solvents with various fractions of poor solvent (i.e., water) to investigate the AIPE effects. Since both **L** and **S** have installed multiple ethylene glycol chains for enhanced solubility in aqueous solutions, they did not show immediate precipitation with a high fraction of water. When the fraction of water was increased, the UV−vis absorption spectra of both **L** and **S** (Figure S67) displayed a rise in the absorption tail around 480 nm, indicating growth of the ^{3}MMLCT transition due to Pt···Pt interaction[30d,39]

Both the ligand **L** and the supramolecule **S** showed weak emission in pure acetonitrile with increasing fraction of water as the poor solvent; **S** exhibited stronger emission in its aggregation state due to the cooperative effect from the Pt(II) motif and ⟨tpy−Cd(II)−tpy⟩ units (Figure 5a and 5b). Furthermore, in the deoxygenated solvent without oxygen quenching for the phosphorescence, supramolecule **S** exhibited significantly enhanced AIPE compared to ligand **L**, i.e., the maximum in emission intensity reached 3.1-fold enhancement for **S** but only 1.3-fold increase for **L** (Figure 5b and 5e). In addition, the AIPE behavior was well maintained along with the increasing fraction of water from 0% to 50%. However,

https://dx.doi.org/10.1021/jacs.0c06680
J. Am. Chem. Soc. XXXX, XXX, XXX−XXX

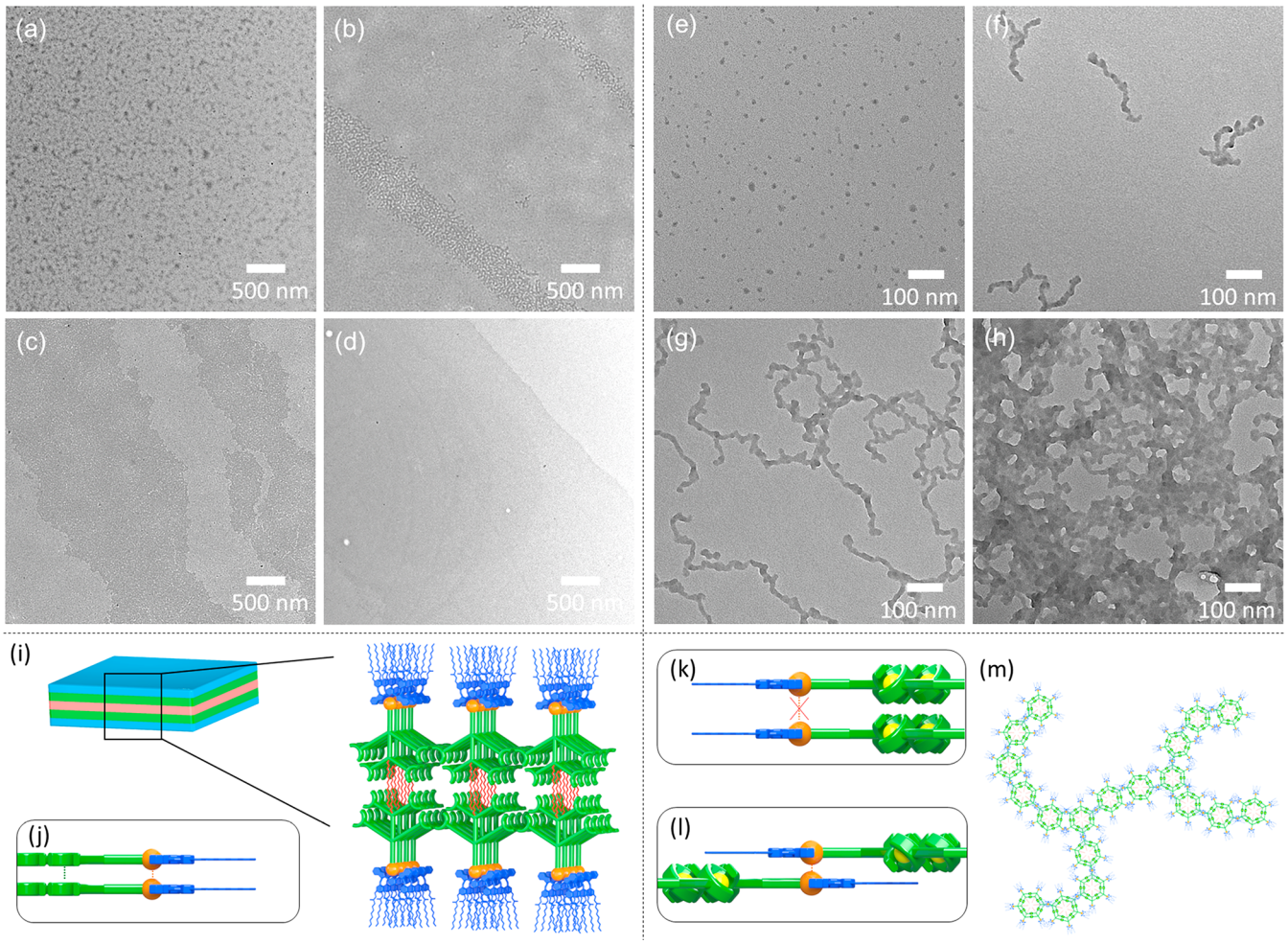

Figure 6. TEM images of **L** and **S** aggregates. TEM images of the aggregates of **L** formed in acetonitrile/water mixtures containing (a) 20%, (b) 40%, (c) 60%, and (d) 80% water and aggregates of **S** formed in acetonitrile/water mixtures containing (e) 20%, (f) 40%, (g) 60%, and (h) 80% water. (i) Proposed formation of sheet-like aggregates by **L**. (j) Proposed Pt···Pt interaction and $\pi-\pi$ stacking between ligands with face-to-face direction. (m) Worm-like aggregates of **S**. (k) Unfavorable face-to-face stacking. (l) Proposed head-to-tail Pt···Pt interaction bridging supramolecules without ring stacking.

further increasing the poor solvent fraction (from 60% to 90%) resulted in a decrease of the phosphorescent intensity. Due to the poor solubility of **L** and **S** in water, we observed large aggregates formed in the solutions with high water fractions after the deoxygenating process. Also, precipitate formation caused the decrement of phosphorescent intensity.

For further comparison and investigation of the AIPE mechanism, supramolecule **C** without Pt(II) motif was constructed (see detailed characterization in Figures S39–S44, S61, and S62) by assembling **A** and Cd(II) directly (Scheme S4). The emission enhancement was also observed by increasing the fraction of water (Figure S69a), suggesting the AIE feature of Cd(II)–tpy-based supramolecules. However, **C** exhibited a short-lived emission of less than 5 ns, and no further enhancements were observed with deoxygenated solvent (Figure S69b), indicating that this emission was fluorescence only.

Interestingly, variations in emission spectra were observed using different gases to deoxygenate the solvent (Figure S70). It was found that CO_2 can further trigger substantial enhancements in emission intensity compared with the results in nondeoxygenated solvent (ca. 5.5-fold increase in the case of **S**, and 1.8-fold increase in the case of **L**). For comparison, N_2 brought about a weaker enhancement for **S** and **L**, i.e., 3.1- and 1.3-fold increase, respectively. We speculated that CO_2 might have weak interactions with Pt(II),[40] since CO_2 has a kinetic diameter of 3.3 Å, which is very close to the ideal distance between Pt atoms in the Pt···Pt interaction (3.5 Å). As such, CO_2 might strengthen the Pt···Pt interactions between supramolecules with a higher RIR effect, leading to an increased emission. In addition, **S** exhibited more significant responses to different gases than **L**, perhaps due to the cooperative effect of multiple Pt(II) centers within the large supramolecular architectures. This property may lead to a potential application for gas sensing.[41]

Morphology studies of aggregates were generally used for evaluating aggregation behaviors and investigating the AIE or AIPE mechanism. Dynamic light scattering (DLS) and TEM were utilized to further elucidate the relationship between the luminescent properties and the aggregation of the ligand **L** and supramolecule **S**. The DLS results (Figure S71) showed the average hydrodynamic diameters (D_h) of the aggregations of **L** and **S** were increased with the increment of the water fraction. Also, the TEM images (Figure 6a–d) showed that **L** aggregated into a layered nanosheet structure in acetonitrile/water, and the size of the sheet was increased with the

https://dx.doi.org/10.1021/jacs.0c06680
J. Am. Chem. Soc. XXXX, XXX, XXX–XXX

increment of water portion. In contrast, **S** aggregated into worm-like structures (Figure 6e–h). With the increase of the water fraction, the length of the worm-like aggregates extended and finally became a cross-linked structure. These results agreed well with the AIPE effect observed in acetonitrile/water solvent.

It is interesting to observe the tremendously different aggregation morphologies of **L** and **S**. To gain further insight into the aggregation mechanism, different solvent mixtures were used to investigate their aggregation behaviors. Compared with the layered structure observed in the CH_3CN/water system, **L** formed spherical aggregates with diameters around 100 nm in DMF/Et_2O solution, and larger spherical structures could be observed in the DMF/i-Pr_2O system (Figure S72). The difference between the sheet and the sphere is possibly due to the long hydrophobic/hydrophilic chains decorated on the inner and outer rims of the ligand performing differently in aqueous/nonaqueous solutions. According to the observation, we postulated that both the Pt···Pt interaction and $\pi-\pi$ stacking might work simultaneously to organize ligand **L** with a face-to-face direction (Figure 6j).

In a sharp contrast, after coordinating with Cd(II), the metallosupramolecule **S** did not aggregate into spherical/layered morphologies as **L** or a tubular structure as the unfunctionalized concentric hexagons.[23h] Instead, the amorphous worm-like structure was the only morphology observed in several different solvent systems (Figure S73). We speculated that the entire concentric hexagon core played an essential role in regulating the aggregating behavior of the Pt–Pt interaction and determining the final morphology of the hierarchical self-assembly. Since the ideal distance between the Pt atoms in the Pt···Pt interaction is reported to be around 3.5 Å,[42] the bulky octahedral coordination of ⟨tpy–Cd(II)–tpy⟩ with a height of 10 Å, as measured from STM, can effectively prohibit formation of $\pi-\pi$ stacking and block the Pt–Pt interaction from the face-to-face orientation (Figure 6k) but force the Pt–Pt interaction to a head-to-tail way (Figure 6l). The emissive behavior of individual components (Pt and tpy) was retained in supramolecule **S**, which displayed enhanced phosphorescent properties during aggregation than individual components.

CONCLUSIONS

In summary, a giant but discrete concentric metallosupramolecule with six well-arrayed alkynyl–platinum(II) bzimpy groups was assembled through rational design to enrich the library of phosphorescent metallosupramolecules, which still remain in its infancy. The cyclic structure was clearly visualized by STM imaging at submolecular resolution. With the Pt(II) motifs installed, the functionalized ligand and the metallosupramolecule exhibited room-temperature phosphorescence with lifetimes of 270 and 218 ns, respectively. With the AIE enhancement from the ⟨tpy–Cd(II)–tpy⟩ coordination, supramolecule **S** exhibited conspicuously stronger AIPE compared to ligand **L**. In addition, both the ligand and the supramolecule exhibited significant responses to CO_2 gas, indicating the potential existence of weak interaction between gas molecules and aggregates. Regarding the aggregation behaviors driven by intermolecular interactions, the ligand could aggregate into layered and spherical structures in different solvent systems, while the supramolecule could only aggregate into a worm-like structure and gel at high concentration. Our endeavors expand the scope of discrete phosphorescent materials into dimensions beyond 10 nm and will shed light on the development of novel phosphorescent materials that combine the advantages from small molecules and polymers, i.e., precise functions, a high level of sophistication, and facile device fabrication.

ASSOCIATED CONTENT

Supporting Information

The Supporting Information is available free of charge at https://pubs.acs.org/doi/10.1021/jacs.0c06680.

Synthetic details; ligands and complexes characterization including ^{1}H NMR, ^{13}C NMR, 2D COSY, 2D NOESY, ESI-MS, TWIM-MS, UV–vis, TEM (PDF)

Compound **14** (CIF)

AUTHOR INFORMATION

Corresponding Author

Xiaopeng Li – *College of Chemistry and Environmental Engineering, Shenzhen University, Shenzhen 518055, China;* orcid.org/0000-0001-9655-9551; Email: xiaopengli@szu.edu.cn

Authors

Yiming Li – *College of Chemistry and Environmental Engineering, Shenzhen University, Shenzhen 518055, China; Department of Chemistry, University of South Florida, Tampa, Florida 33620, United States*

Gui-Fei Huo – *Shanghai Key Laboratory of Green Chemistry and Chemical Processes, Department of Chemistry, East China Normal University, Shanghai 200062, China*

Bingqing Liu – *Department of Chemistry and Biochemistry, North Dakota State University, Fargo, North Dakota 58105, United States*

Bo Song – *Department of Chemistry, Northwestern University, Evanston, Illinois 60208, United States*

Yuan Zhang – *Department of Physics, Old Dominion University, Norfolk, Virginia 23529, United States*

Xiaomin Qian – *Department of Chemistry, University of South Florida, Tampa, Florida 33620, United States*

Heng Wang – *College of Chemistry and Environmental Engineering, Shenzhen University, Shenzhen 518055, China*

Guang-Qiang Yin – *College of Chemistry and Environmental Engineering, Shenzhen University, Shenzhen 518055, China*

Alexander Filosa – *Department of Chemistry, University of South Florida, Tampa, Florida 33620, United States*

Wenfang Sun – *Department of Chemistry and Biochemistry, North Dakota State University, Fargo, North Dakota 58105, United States;* orcid.org/0000-0003-3608-611X

Saw Wai Hla – *Nanoscience and Technology Division, Argonne National Laboratory, Lemont, Illinois 60439, United States*

Hai-Bo Yang – *Shanghai Key Laboratory of Green Chemistry and Chemical Processes, Department of Chemistry, East China Normal University, Shanghai 200062, China;* orcid.org/0000-0003-4926-1618

Complete contact information is available at: https://pubs.acs.org/10.1021/jacs.0c06680

Author Contributions

[‖]Y.L. and G.-F. H. contributed equally.

Notes

The authors declare no competing financial interest.

https://dx.doi.org/10.1021/jacs.0c06680
J. Am. Chem. Soc. XXXX, XXX, XXX–XXX

■ ACKNOWLEDGMENTS

This research was supported by Shenzhen University and the University of South Florida. Use of the Center for Nanoscale Materials, an Office of Science user facility, was supported by the U.S. Department of Energy, Office of Science, Office of Basic Energy Sciences, under Contract No. DE-AC02-06CH11357.

■ REFERENCES

(1) (a) Ruben, M.; Rojo, J.; Romero-Salguero, F. J.; Uppadine, L. H.; Lehn, J.-M. Grid-type metal ion architectures: Functional metallosupramolecular arrays. *Angew. Chem., Int. Ed.* **2004**, *43* (28), 3644−3662. (b) Fujita, M.; Tominaga, M.; Hori, A.; Therrien, B. Coordination assemblies from a Pd(II)-cornered square complex. *Acc. Chem. Res.* **2005**, *38* (4), 369−378. (c) Chakrabarty, R.; Mukherjee, P. S.; Stang, P. J. Supramolecular coordination: Self-assembly of finite two- and three-dimensional ensembles. *Chem. Rev.* **2011**, *111* (11), 6810−6918. (d) Han, M.; Engelhard, D. M.; Clever, G. H. Self-assembled coordination cages based on banana-shaped ligands. *Chem. Soc. Rev.* **2014**, *43* (6), 1848−1860. (e) Chen, L.-J.; Yang, H.-B.; Shionoya, M. Chiral metallosupramolecular architectures. *Chem. Soc. Rev.* **2017**, *46* (9), 2555−2576. (f) Rizzuto, F. J.; von Krbek, L. K. S.; Nitschke, J. R. Strategies for binding multiple guests in metal-organic cages. *Nat. Rev. Chem.* **2019**, *3* (4), 204−222.

(2) (a) Sun, S.-S.; Lees, A. J. Transition metal based supramolecular systems: synthesis, photophysics, photochemistry and their potential applications as luminescent anion chemosensors. *Coord. Chem. Rev.* **2002**, *230* (1), 171−192. (b) Thanasekaran, P.; Liao, R.-T.; Liu, Y.-H.; Rajendran, T.; Rajagopal, S.; Lu, K.-L. Metal-containing molecular rectangles: synthesis and photophysical properties. *Coord. Chem. Rev.* **2005**, *249* (9), 1085−1110. (c) Cook, T. R.; Vajpayee, V.; Lee, M. H.; Stang, P. J.; Chi, K.-W. Biomedical and biochemical applications of self-assembled metallacycles and metallacages. *Acc. Chem. Res.* **2013**, *46* (11), 2464−2474. (d) Zhang, D.; Ronson, T. K.; Nitschke, J. R. Functional capsules via subcomponent self-assembly. *Acc. Chem. Res.* **2018**, *51* (10), 2423−2436. (e) Goswami, A.; Saha, S.; Biswas, P. K.; Schmittel, M. (Nano)mechanical motion triggered by metal coordination: From functional devices to networked multicomponent catalytic machinery. *Chem. Rev.* **2020**, *120* (1), 125−199.

(3) (a) Neelakandan, P. P.; Jiménez, A.; Nitschke, J. R. Fluorophore incorporation allows nanomolar guest sensing and white-light emission in M_4L_6 cage complexes. *Chem. Sci.* **2014**, *5* (3), 908−915. (b) Liu, C.-L.; Zhang, R.-L.; Lin, C.-S.; Zhou, L.-P.; Cai, L.-X.; Kong, J.-T.; Yang, S.-Q.; Han, K.-L.; Sun, Q.-F. Intraligand charge transfer sensitization on self-assembled europium tetrahedral cage leads to dual-selective luminescent sensing toward anion and cation. *J. Am. Chem. Soc.* **2017**, *139* (36), 12474−12479. (c) Zhou, Z.; Chen, D. G.; Saha, M. L.; Wang, H.; Li, X.; Chou, P. T.; Stang, P. J. Designed conformation and fluorescence properties of self-assembled phenazine-cored platinum(II) metallacycles. *J. Am. Chem. Soc.* **2019**, *141* (13), 5535−5543. (d) Zhang, Z.; Zhao, Z.; Wu, L.; Lu, S.; Ling, S.; Li, G.; Xu, L.; Ma, L.; Hou, Y.; Wang, X.; Li, X.; He, G.; Wang, K.; Zou, B.; Zhang, M. Emissive platinum(II) cages with reverse fluorescence resonance energy transfer for multiple sensing. *J. Am. Chem. Soc.* **2020**, *142* (5), 2592−2600.

(4) (a) Wu, K.; Li, K.; Hou, Y.-J.; Pan, M.; Zhang, L.-Y.; Chen, L.; Su, C.-Y. Homochiral D4-symmetric metal-organic cages from stereogenic Ru(II) metalloligands for effective enantioseparation of atropisomeric molecules. *Nat. Commun.* **2016**, *7* (1), 10487. (b) Guo, J.; Fan, Y. Z.; Lu, Y. L.; Zheng, S. P.; Su, C. Y. Visible-light photocatalysis of asymmetric [2 + 2] cycloaddition in cage-confined nanospace merging chirality with triplet-state photosensitization. *Angew. Chem.* **2020**, *132* (22), 8739−8747.

(5) (a) Zhang, M.; Li, S.; Yan, X.; Zhou, Z.; Saha, M. L.; Wang, Y.-C.; Stang, P. J. Fluorescent metallacycle-cored polymers via covalent linkage and their use as contrast agents for cell imaging. *Proc. Natl. Acad. Sci. U. S. A.* **2016**, *113* (40), 11100. (b) Zhou, J.; Zhang, Y.; Yu, G.; Crawley, M. R.; Fulong, C. R. P.; Friedman, A. E.; Sengupta, S.; Sun, J.; Li, Q.; Huang, F.; Cook, T. R. Highly emissive self-assembled BODIPY-platinum supramolecular triangles. *J. Am. Chem. Soc.* **2018**, *140* (24), 7730−7736. (c) Burke, B. P.; Grantham, W.; Burke, M. J.; Nichol, G. S.; Roberts, D.; Renard, I.; Hargreaves, R.; Cawthorne, C.; Archibald, S. J.; Lusby, P. J. Visualizing kinetically robust Co_4L_6 assemblies *in vivo*: spect imaging of the encapsulated $[^{99m}Tc]TcO_4^-$ anion. *J. Am. Chem. Soc.* **2018**, *140* (49), 16877−16881. (d) Wu, L.; Ishigaki, Y.; Hu, Y.; Sugimoto, K.; Zeng, W.; Harimoto, T.; Sun, Y.; He, J.; Suzuki, T.; Jiang, X.; Chen, H.-Y.; Ye, D. H_2S-activatable near-infrared afterglow luminescent probes for sensitive molecular imaging in vivo. *Nat. Commun.* **2020**, *11* (1), 446. (e) Yu, G.; Cook, T. R.; Li, Y.; Yan, X.; Wu, D.; Shao, L.; Shen, J.; Tang, G.; Huang, F.; Chen, X.; Stang, P. J. Tetraphenylethene-based highly emissive metallacage as a component of theranostic supramolecular nanoparticles. *Proc. Natl. Acad. Sci. U. S. A.* **2016**, *113* (48), 13720.

(6) (a) Chepelin, O.; Ujma, J.; Wu, X.; Slawin, A. M. Z.; Pitak, M. B.; Coles, S. J.; Michel, J.; Jones, A. C.; Barran, P. E.; Lusby, P. J. Luminescent, enantiopure, phenylatopyridine iridium-based coordination capsules. *J. Am. Chem. Soc.* **2012**, *134* (47), 19334−19337. (b) Kaloudi-Chantzea, A.; Karakostas, N.; Pitterl, F.; Raptopoulou, C. P.; Glezos, N.; Pistolis, G. Efficient supramolecular synthesis of a robust circular light-harvesting Bodipy-dye based array. *Chem. Commun.* **2012**, *48* (100), 12213−12215.

(7) (a) Yu, G.; Yu, S.; Saha, M. L.; Zhou, J.; Cook, T. R.; Yung, B. C.; Chen, J.; Mao, Z.; Zhang, F.; Zhou, Z.; Liu, Y.; Shao, L.; Wang, S.; Gao, C.; Huang, F.; Stang, P. J.; Chen, X. A discrete organoplatinum-(II) metallacage as a multimodality theranostic platform for cancer photochemotherapy. *Nat. Commun.* **2018**, *9* (1), 4335. (b) Qin, Y.; Chen, L.-J.; Dong, F.; Jiang, S.-T.; Yin, G.-Q.; Li, X.; Tian, Y.; Yang, H.-B. Light-controlled generation of singlet oxygen within a discrete dual-stage metallacycle for cancer therapy. *J. Am. Chem. Soc.* **2019**, *141* (22), 8943−8950. (c) Zhou, Z.; Liu, J.; Huang, J.; Rees, T. W.; Wang, Y.; Wang, H.; Li, X.; Chao, H.; Stang, P. J. A self-assembled Ru-Pt metallacage as a lysosome-targeting photosensitizer for 2-photon photodynamic therapy. *Proc. Natl. Acad. Sci. U. S. A.* **2019**, *116* (41), 20296.

(8) (a) Saha, M. L.; Yan, X.; Stang, P. J. Photophysical properties of organoplatinum(II) compounds and derived self-assembled metallacycles and metallacages: Fluorescence and its applications. *Acc. Chem. Res.* **2016**, *49* (11), 2527−2539. (b) Kitchen, J. A. Lanthanide-based self-assemblies of 2,6-pyridyldicarboxamide ligands: Recent advances and applications as next-generation luminescent and magnetic materials. *Coord. Chem. Rev.* **2017**, *340*, 232−246. (c) Xuan, W.; Zhang, M.; Liu, Y.; Chen, Z.; Cui, Y. A chiral quadruple-stranded helicate cage for enantioselective recognition and separation. *J. Am. Chem. Soc.* **2012**, *134* (16), 6904−6907. (d) Lewis, J. E. M.; Elliott, A. B. S.; McAdam, C. J.; Gordon, K. C.; Crowley, J. D. 'Click' to functionalise: synthesis, characterisation and enhancement of the physical properties of a series of exo- and endo-functionalised Pd_2L_4 nanocages. *Chem. Sci.* **2014**, *5* (5), 1833−1843. (e) Dalton, D. M.; Ellis, S. R.; Nichols, E. M.; Mathies, R. A.; Toste, F. D.; Bergman, R. G.; Raymond, K. N. Supramolecular $Ga_4L_6^{12-}$ cage photosensitizes 1,3-rearrangement of encapsulated guest via photoinduced electron transfer. *J. Am. Chem. Soc.* **2015**, *137* (32), 10128−10131. (f) Yamashina, M.; Sartin, M. M.; Sei, Y.; Akita, M.; Takeuchi, S.; Tahara, T.; Yoshizawa, M. Preparation of highly fluorescent host-guest complexes with tunable color upon encapsulation. *J. Am. Chem. Soc.* **2015**, *137* (29), 9266−9269. (g) Rota Martir, D.; Zysman-Colman, E. Photoactive supramolecular cages incorporating Ru(II) and Ir(III) metal complexes. *Chem. Commun.* **2019**, *55* (2), 139−158. (h) Hu, Y. X.; Hao, X.; Xu, L.; Xie, X.; Xiong, B.; Hu, Z.; Sun, H.; Yin, G. Q.; Li, X.; Peng, H.; Yang, H. B. Construction of supramolecular liquid-crystalline metallacycles for holographic storage of colored images. *J. Am. Chem. Soc.* **2020**, *142* (13), 6285−6294. (i) Chen, L.; Chen, C.; Sun, Y.; Lu, S.; Huo, H.; Tan, T.; Li, A.; Li, X.; Ungar, G.; Liu, F.; Zhang, M. Luminescent metallacycle-cored liquid crystals induced by metal coordination. *Angew. Chem.* **2020**, *132* (25), 10229−10236. (j) Bogie, P. M.; Miller, T. F.; Hooley, R. J. Synthesis and applications of endohedrally functionalized metal-ligand cage

https://dx.doi.org/10.1021/jacs.0c06680
J. Am. Chem. Soc. XXXX, XXX, XXX−XXX

complexes. *Isr. J. Chem.* **2019**, *59* (3−4), 130−139. (k) Samanta, S. K.; Isaacs, L. Biomedical applications of metal organic polygons and polyhedra (MOPs). *Coord. Chem. Rev.* **2020**, *410*, 213181.

(9) (a) Gao, G.-F.; Li, M.; Zhan, S.-Z.; Lv, Z.; Chen, G.-h.; Li, D. Confined metallophilicity within a coordination prism. *Chem. - Eur. J.* **2011**, *17* (15), 4113−4117. (b) Li, X.-Z.; Zhou, L.-P.; Yan, L.-L.; Yuan, D.-Q.; Lin, C.-S.; Sun, Q.-F. Evolution of luminescent supramolecular lanthanide $M_{2n}L_{3n}$ complexes from helicates and tetrahedra to cubes. *J. Am. Chem. Soc.* **2017**, *139* (24), 8237−8244.

(10) Rota Martir, D.; Escudero, D.; Jacquemin, D.; Cordes, D. B.; Slawin, A. M. Z.; Fruchtl, H. A.; Warriner, S. L.; Zysman-Colman, E. Homochiral emissive Λ_8- and Δ_8-$[Ir_8Pd_4]^{16+}$ supramolecular cages. *Chem. - Eur. J.* **2017**, *23* (57), 14358−14366.

(11) (a) Ono, K.; Klosterman, J. K.; Yoshizawa, M.; Sekiguchi, K.; Tahara, T.; Fujita, M. ON/OFF red emission from azaporphine in a coordination cage in water. *J. Am. Chem. Soc.* **2009**, *131* (35), 12526−12527. (b) August, D. P.; Nichol, G. S.; Lusby, P. J. Maximizing coordination capsule-guest polar interactions in apolar solvents reveals significant binding. *Angew. Chem., Int. Ed.* **2016**, *55* (48), 15022−15026. (c) Taylor, C. G.; Piper, J. R.; Ward, M. D. Binding of chemical warfare agent simulants as guests in a coordination cage: contributions to binding and a fluorescence-based response. *Chem. Commun.* **2016**, *52* (37), 6225−6228.

(12) (a) Yan, X.; Wang, H.; Hauke, C. E.; Cook, T. R.; Wang, M.; Saha, M. L.; Zhou, Z.; Zhang, M.; Li, X.; Huang, F.; Stang, P. J. A suite of tetraphenylethylene-based discrete organoplatinum(II) metallacycles: controllable structure and stoichiometry, aggregation-induced emission, and nitroaromatics sensing. *J. Am. Chem. Soc.* **2015**, *137* (48), 15276−15286. (b) Yan, X.; Cook, T. R.; Wang, P.; Huang, F.; Stang, P. J. Highly emissive platinum(II) metallacages. *Nat. Chem.* **2015**, *7* (4), 342−348. (c) Lu, C.; Zhang, M.; Tang, D.; Yan, X.; Zhang, Z.; Zhou, Z.; Song, B.; Wang, H.; Li, X.; Yin, S.; Sepehrpour, H.; Stang, P. J. Fluorescent metallacage-core supramolecular polymer gel formed by orthogonal metal coordination and host-guest interactions. *J. Am. Chem. Soc.* **2018**, *140* (24), 7674−7680. (d) Dong, J.; Pan, Y.; Wang, H.; Yang, K.; Liu, L.; Qiao, Z.; Yuan, Y. D.; Peh, S. B.; Zhang, J.; Shi, L.; Liang, H.; Han, Y.; Li, X.; Jiang, J.; Liu, B.; Zhao, D. Self-assembly of highly stable zirconium(IV) coordination cages with aggregation induced emission molecular rotors for live-cell imaging. *Angew. Chem., Int. Ed.* **2020**, *59*, 10151. (e) Dong, J.; Pan, Y.; Wang, H.; Yang, K.; Liu, L.; Qiao, Z.; Yuan, Y. D.; Peh, S. B.; Zhang, J.; Shi, L.; Liang, H.; Han, Y.; Li, X.; Jiang, J.; Liu, B.; Zhao, D. Self-assembly of highly stable zirconium(IV) coordination cages with aggregation induced emission molecular rotors for live-cell imaging. *Angew. Chem., Int. Ed.* **2020**, *59* (25), 10151−10159.

(13) (a) Zhang, M.; Saha, M. L.; Wang, M.; Zhou, Z.; Song, B.; Lu, C.; Yan, X.; Li, X.; Huang, F.; Yin, S.; Stang, P. J. Multicomponent platinum(II) cages with tunable emission and amino acid sensing. *J. Am. Chem. Soc.* **2017**, *139* (14), 5067−5074. (b) Musser, A. J.; Neelakandan, P. P.; Richter, J. M.; Mori, H.; Friend, R. H.; Nitschke, J. R. Excitation energy delocalization and transfer to guests within M_4L_6 cage frameworks. *J. Am. Chem. Soc.* **2017**, *139* (34), 12050−12059. (c) Käseborn, M.; Holstein, J. J.; Clever, G. H.; Lützen, A. A rotaxane-like cage-in-ring structural motif for a metallosupramolecular Pd_6L_{12} aggregate. *Angew. Chem., Int. Ed.* **2018**, *57* (37), 12171−12175.

(14) (a) Wang, J.; He, C.; Wu, P.; Wang, J.; Duan, C. An amide-containing metal-organic tetrahedron responding to a spin-trapping reaction in a fluorescent enhancement manner for biological imaging of NO in living cells. *J. Am. Chem. Soc.* **2011**, *133* (32), 12402−12405. (b) Zhu, J. L.; Xu, L.; Ren, Y. Y.; Zhang, Y.; Liu, X.; Yin, G. Q.; Sun, B.; Cao, X.; Chen, Z.; Zhao, X. L.; Tan, H.; Chen, J.; Li, X.; Yang, H. B. Switchable organoplatinum metallacycles with high quantum yields and tunable fluorescence wavelengths. *Nat. Commun.* **2019**, *10* (1), 4285.

(15) Chang, X.; Zhou, Z.; Shang, C.; Wang, G.; Wang, Z.; Qi, Y.; Li, Z. Y.; Wang, H.; Cao, L.; Li, X.; Fang, Y.; Stang, P. J. Coordination-driven self-assembled metallacycles incorporating pyrene: Fluorescence mutability, tunability, and aromatic amine sensing. *J. Am. Chem. Soc.* **2019**, *141* (4), 1757−1765.

(16) (a) Mahata, K.; Frischmann, P. D.; Würthner, F. Giant electroactive M_4L_6 tetrahedral host self-assembled with Fe(II) vertices and perylene bisimide dye edges. *J. Am. Chem. Soc.* **2013**, *135* (41), 15656−15661. (b) Frischmann, P. D.; Kunz, V.; Würthner, F. Bright fluorescence and host-guest sensing with a nanoscale M_4L_6 tetrahedron accessed by self-assembly of zinc-imine chelate vertices and perylene bisimide edges. *Angew. Chem., Int. Ed.* **2015**, *54* (25), 7285−7289.

(17) (a) Li, K.; Zhang, L.-Y.; Yan, C.; Wei, S.-C.; Pan, M.; Zhang, L.; Su, C.-Y. Stepwise assembly of $Pd_6(RuL_3)_8$ nanoscale rhombododecahedral metal-organic cages via metalloligand strategy for guest trapping and protection. *J. Am. Chem. Soc.* **2014**, *136* (12), 4456−4459. (b) Chen, S.; Li, K.; Zhao, F.; Zhang, L.; Pan, M.; Fan, Y.-Z.; Guo, J.; Shi, J.; Su, C.-Y. A metal-organic cage incorporating multiple light harvesting and catalytic centres for photochemical hydrogen production. *Nat. Commun.* **2016**, *7* (1), 13169.

(18) (a) Stomeo, F.; Lincheneau, C.; Leonard, J. P.; O'Brien, J. E.; Peacock, R. D.; McCoy, C. P.; Gunnlaugsson, T. Metal-directed synthesis of enantiomerially pure dimetallic lanthanide luminescent triple-stranded helicates. *J. Am. Chem. Soc.* **2009**, *131* (28), 9636−9637. (b) Yeung, C.-T.; Chan, W. T. K.; Yan, S.-C.; Yu, K.-L.; Yim, K.-H.; Wong, W.-T.; Law, G.-L. Lanthanide supramolecular helical diastereoselective breaking induced by point chirality: mixture or P-helix, M-helix. *Chem. Commun.* **2015**, *51* (3), 592−595. (c) Yan, L.-L.; Tan, C.-H.; Zhang, G.-L.; Zhou, L.-P.; Bünzli, J.-C.; Sun, Q.-F. Stereocontrolled self-assembly and self-sorting of luminescent europium tetrahedral cages. *J. Am. Chem. Soc.* **2015**, *137* (26), 8550−8555. (d) Guo, X.-Q.; Zhou, L.-P.; Cai, L.-X.; Sun, Q.-F. Self-assembled bright luminescent lanthanide-organic polyhedra for ratiometric temperature sensing. *Chem. - Eur. J.* **2018**, *24* (27), 6936−6940.

(19) Schmittel, M.; Shu, Q.; Cinar, M. E. Tuning the wavelength of electrochemiluminescence by anodic potential: a design using non-Kekulé-structured iridium-ruthenium luminophores. *Dalton Trans.* **2012**, *41* (20), 6064−6068.

(20) (a) Goeb, S.; Prusakova, V.; Wang, X.; Vézinat, A.; Sallé, M.; Castellano, F. N. Phosphorescent self-assembled Pt^{II} tetranuclear metallocycles. *Chem. Commun.* **2011**, *47* (15), 4397−4399. (b) Pollock, J. B.; Schneider, G. L.; Cook, T. R.; Davies, A. S.; Stang, P. J. Tunable visible light emission of self-assembled rhomboidal metallacycles. *J. Am. Chem. Soc.* **2013**, *135* (37), 13676−13679. (c) Zhang, Y.; Fulong, C. R. P.; Hauke, C. E.; Crawley, M. R.; Friedman, A. E.; Cook, T. R. Photophysical enhancement of triplet emitters by coordination-driven self-assembly. *Chem. - Eur. J.* **2017**, *23* (19), 4532−4536. (d) Zhou, Z.; Hauke, C. E.; Song, B.; Li, X.; Stang, P. J.; Cook, T. R. Understanding the effects of coordination and self-assembly on an emissive phenothiazine. *J. Am. Chem. Soc.* **2019**, *141* (8), 3717−3722. (e) Bhattacharyya, S.; Chowdhury, A.; Saha, R.; Mukherjee, P. S. Multifunctional self-assembled macrocycles with enhanced emission and reversible photochromic behavior. *Inorg. Chem.* **2019**, *58* (6), 3968−3981. (f) Pollock, J. B.; Cook, T. R.; Schneider, G. L.; Lutterman, D. A.; Davies, A. S.; Stang, P. J. Photophysical properties of endohedral amine-functionalized bis(phosphine) Pt(II) complexes as models for emissive metallacycles. *Inorg. Chem.* **2013**, *52* (16), 9254−9265. (g) Acharyya, K.; Bhattacharyya, S.; Sepehrpour, H.; Chakraborty, S.; Lu, S.; Shi, B.; Li, X.; Mukherjee, P. S.; Stang, P. J. Self-assembled fluorescent Pt(II) metallacycles as artificial light-harvesting systems. *J. Am. Chem. Soc.* **2019**, *141* (37), 14565−14569.

(21) (a) Jiang, X.-F.; Hau, F. K.-W.; Sun, Q.-F.; Yu, S.-Y.; Yam, V. W.-W. From {AuI···AuI}-coupled cages to the cage-built 2-D {AuI···AuI} arrays: AuI···AuINbonding interaction driven self-assembly and their AgI sensing and photo-switchable behavior. *J. Am. Chem. Soc.* **2014**, *136* (31), 10921−10929. (b) Li, Y.; An, Y.-Y.; Fan, J.-Z.; Liu, X.-X.; Li, X.; Hahn, F. E.; Wang, Y.-Y.; Han, Y.-F. Strategy for the construction of diverse poly-NHC-derived assemblies and their photoinduced transformations. *Angew. Chem., Int. Ed.* **2020**, *59* (25), 10073−10080. (c) Sun, L.-Y.; Feng, T.; Das, R.; Hahn, F. E.;

https://dx.doi.org/10.1021/jacs.0c06680
J. Am. Chem. Soc. XXXX, XXX, XXX−XXX

Han, Y.-F. Synthesis, characterization, and properties of tetraphenylethylene-based tetrakis-NHC ligands and their metal complexes. *Chem. - Eur. J.* **2019**, *25* (41), 9764−9770.

(22) (a) Wu, S.-Y.; Guo, X.-Q.; Zhou, L.-P.; Sun, Q.-F. Fine-tuned visible and near-infrared luminescence on self-assembled lanthanide-organic tetrahedral cages with triazole-based chelates. *Inorg. Chem.* **2019**, *58* (10), 7091−7098. (b) Zhang, Y.; Crawley, M. R.; Hauke, C. E.; Friedman, A. E.; Cook, T. R. Phosphorescent decanuclear bimetallic Pt_6M_4 (M = Zn, Fe) tetrahedral cages. *Inorg. Chem.* **2017**, *56* (8), 4258−4262. (c) Zhang, Y.; Cox, J. M.; Friedman, A. E.; Benedict, J. B.; Cook, T. R. Phosphorescent organoplatinum(II) D_2A_2 metallacycles: synthesis, self-assembly, and photophysical properties. *J. Coord. Chem.* **2016**, *69* (11−13), 1914−1923.

(23) (a) Chakraborty, S.; Newkome, G. R. Terpyridine-based metallosupramolecular constructs: tailored monomers to precise 2D-motifs and 3D-metallocages. *Chem. Soc. Rev.* **2018**, *47* (11), 3991−4016. (b) Newkome, G. R.; Wang, P. S.; Moorefield, C. N.; Cho, T. J.; Mohapatra, P. P.; Li, S. N.; Hwang, S. H.; Lukoyanova, O.; Echegoyen, L.; Palagallo, J. A.; Iancu, V.; Hla, S. W. Nanoassembly of a fractal polymer: A molecular "Sierpinski hexagonal gasket. *Science* **2006**, *312* (5781), 1782−1785. (c) Fu, J.-H.; Lee, Y.-H.; He, Y.-J.; Chan, Y.-T. Facile self-assembly of metallo-supramolecular ring-in-ring and spiderweb structures using multivalent terpyridine ligands. *Angew. Chem., Int. Ed.* **2015**, *54* (21), 6231−6235. (d) Xie, T. Z.; Guo, K.; Guo, Z. H.; Gao, W. Y.; Wojtas, L.; Ning, G. H.; Huang, M. J.; Lu, X. C.; Li, J. Y.; Liao, S. Y.; Chen, Y. S.; Moorefield, C. N.; Saunders, M. J.; Cheng, S. Z. D.; Wesdemiotis, C.; Newkome, G. R. Precise molecular fission and fusion: Quantitative self-assembly and chemistry of a metallo-cuboctahedron. *Angew. Chem., Int. Ed.* **2015**, *54* (32), 9224−9229. (e) Li, Y.; Jiang, Z.; Wang, M.; Yuan, J.; Liu, D.; Yang, X.; Chen, M.; Yan, J.; Li, X.; Wang, P. Giant, hollow 2D metalloarchitecture: Stepwise self-assembly of a hexagonal supramolecular nut. *J. Am. Chem. Soc.* **2016**, *138* (31), 10041−10046. (f) Wang, S.-Y.; Fu, J.-H.; Liang, Y.-P.; He, Y.-J.; Chen, Y.-S.; Chan, Y.-T. Metallo-supramolecular self-assembly of a multicomponent ditrigon based on complementary terpyridine ligand pairing. *J. Am. Chem. Soc.* **2016**, *138* (11), 3651−3654. (g) Jiang, Z.; Li, Y.; Wang, M.; Song, B.; Wang, K.; Sun, M.; Liu, D.; Li, X.; Yuan, J.; Chen, M.; Guo, Y.; Yang, X.; Zhang, T.; Moorefield, C. N.; Newkome, G. R.; Xu, B.; Li, X.; Wang, P. Self-assembly of a supramolecular hexagram and a supramolecular pentagram. *Nat. Commun.* **2017**, *8* (1), 15476. (h) Wang, H.; Qian, X.; Wang, K.; Su, M.; Haoyang, W. W.; Jiang, X.; Brzozowski, R.; Wang, M.; Gao, X.; Li, Y.; Xu, B.; Eswara, P.; Hao, X. Q.; Gong, W.; Hou, J. L.; Cai, J.; Li, X. Supramolecular Kandinsky circles with high antibacterial activity. *Nat. Commun.* **2018**, *9* (1), 1815. (i) Liu, D.; Chen, M.; Li, Y.; Shen, Y.; Huang, J.; Yang, X.; Jiang, Z.; Li, X.; Newkome, G. R.; Wang, P. Vertical assembly of giant double- and triple-decker spoked wheel supramolecular structures. *Angew. Chem., Int. Ed.* **2018**, *57* (43), 14116−14120. (j) Chen, Y.-S.; Solel, E.; Huang, Y.-F.; Wang, C.-L.; Tu, T.-H.; Keinan, E.; Chan, Y.-T. Chemical mimicry of viral capsid self-assembly via corannulene-based pentatopic tectons. *Nat. Commun.* **2019**, *10* (1), 3443. (k) Zhang, Z.; Li, Y.; Song, B.; Zhang, Y.; Jiang, X.; Wang, M.; Tumbleson, R.; Liu, C.; Wang, P.; Hao, X.-Q.; Rojas, T.; Ngo, A. T.; Sessler, J. L.; Newkome, G. R.; Hla, S. W.; Li, X. Intra- and intermolecular self-assembly of a 20-nm-wide supramolecular hexagonal grid. *Nat. Chem.* **2020**, *12*, 468−474.

(24) (a) Constable, E. C. 2,2′:6′,2″-Terpyridines: From chemical obscurity to common supramolecular motifs. *Chem. Soc. Rev.* **2007**, *36* (2), 246−253. (b) Wild, A.; Winter, A.; Schlütter, F.; Schubert, U. S. Advances in the field of π-conjugated 2,2′:6′,2″-terpyridines. *Chem. Soc. Rev.* **2011**, *40* (3), 1459−1511.

(25) (a) Chen, X. G.; Ding, Y. Q.; Cheng, Y. X.; Wang, L. X. Synthesis, spectroscopy and electroluminescence of cadmium(II) polypyridyl complexes. *Synth. Met.* **2010**, *160* (7−8), 625−630. (b) Wang, J. L.; Li, X. P.; Lu, X. C.; Chan, Y. T.; Moorefield, C. N.; Wesdemiotis, C.; Newkome, G. R. Dendron-functionalized bis-(terpyridine)-iron(II) or -cadmium(II) metallomacrocycles: Synthesis, traveling-wave ion-mobility mass spectrometry, and photophysical properties. *Chem. - Eur. J.* **2011**, *17* (17), 4830−4838. (c) Schultz, A.; Cao, Y.; Huang, M. J.; Cheng, S. Z. D.; Li, X. P.; Moorefield, C. N.; Wesdemiotis, C.; Newkome, G. R. Stable, trinuclear Zn(II)- and Cd(II)-metallocycles: TWIM-MS, photophysical properties, and nanofiber formation. *Dalton Trans.* **2012**, *41* (38), 11573−11575. (d) Yin, G. Q.; Wang, H.; Wang, X. Q.; Song, B.; Chen, L. J.; Wang, L.; Hao, X. Q.; Yang, H. B.; Li, X. Self-assembly of emissive supramolecular rosettes with increasing complexity using multitopic terpyridine ligands. *Nat. Commun.* **2018**, *9* (1), 567. (e) Liu, D.; Chen, M.; Li, K.; Li, Z.; Huang, J.; Wang, J.; Jiang, Z.; Zhang, Z.; Xie, T.; Newkome, G. R.; Wang, P. Giant truncated metallo-tetrahedron with unexpected supramolecular aggregation induced emission enhancement. *J. Am. Chem. Soc.* **2020**, *142* (17), 7987−7994.

(26) (a) Luo, J.; Xie, Z.; Lam, J. W. Y.; Cheng, L.; Chen, H.; Qiu, C.; Kwok, H. S.; Zhan, X.; Liu, Y.; Zhu, D.; Tang, B. Z. Aggregation-induced emission of 1-methyl-1,2,3,4,5-pentaphenylsilole. *Chem. Commun.* **2001**, No. 18, 1740−1741. (b) Hong, Y.; Lam, J. W. Y.; Tang, B. Z. Aggregation-induced emission: phenomenon, mechanism and applications. *Chem. Commun.* **2009**, No. 29, 4332−4353. (c) Hong, Y.; Lam, J. W. Y.; Tang, B. Z. Aggregation-induced emission. *Chem. Soc. Rev.* **2011**, *40* (11), 5361−5388. (d) Hu, R.; Leung, N. L. C.; Tang, B. Z. AIE macromolecules: syntheses, structures and functionalities. *Chem. Soc. Rev.* **2014**, *43* (13), 4494−4562. (e) Mei, J.; Leung, N. L. C.; Kwok, R. T. K.; Lam, J. W. Y.; Tang, B. Z. Aggregation-induced emission: Together we shine, united we soar! *Chem. Rev.* **2015**, *115* (21), 11718−11940. (f) Chowdhury, A.; Howlader, P.; Mukherjee, P. S. Aggregation-induced emission of platinum(II) metallacycles and their ability to detect nitroaromatics. *Chem. - Eur. J.* **2016**, *22* (22), 7468−7478. (g) Das, P.; Kumar, A.; Chowdhury, A.; Mukherjee, P. S. Aggregation-induced emission and white luminescence from a combination of π-conjugated donor-acceptor organic luminogens. *ACS Omega* **2018**, *3* (10), 13757−13771. (h) Dong, J.; Li, X.; Zhang, K.; Di Yuan, Y.; Wang, Y.; Zhai, L.; Liu, G.; Yuan, D.; Jiang, J.; Zhao, D. Confinement of aggregation-induced emission molecular rotors in ultrathin two-dimensional porous organic nanosheets for enhanced molecular recognition. *J. Am. Chem. Soc.* **2018**, *140* (11), 4035−4046.

(27) (a) Ott, C.; Ulbricht, C.; Hoogenboom, R.; Schubert, U. S. Metallo-supramolecular materials based on amine-grafting onto polypentafluorostyrene. *Macromol. Rapid Commun.* **2012**, *33* (6−7), 556−561. (b) Fermi, A.; Bergamini, G.; Roy, M.; Gingras, M.; Ceroni, P. Turn-on phosphorescence by metal coordination to a multivalent terpyridine ligand: A new paradigm for luminescent sensors. *J. Am. Chem. Soc.* **2014**, *136* (17), 6395−6400.

(28) (a) Cummings, S. D. Platinum complexes of terpyridine: Synthesis, structure and reactivity. *Coord. Chem. Rev.* **2009**, *253* (3), 449−478. (b) Yam, V. W. W.; Au, V. K. M.; Leung, S. Y. L. Light-emitting self-assembled materials based on d(8) and d(10) transition metal complexes. *Chem. Rev.* **2015**, *115* (15), 7589−7728. (c) Chowdhury, A.; Howlader, P.; Mukherjee, P. S. Mechano-fluorochromic Pt^{II} luminogen and its cysteine recognition. *Chem. - Eur. J.* **2016**, *22* (4), 1424−1434.

(29) (a) Castellano, F. N.; Pomestchenko, I. E.; Shikhova, E.; Hua, F.; Muro, M. L.; Rajapakse, N. Photophysics in bipyridyl and terpyridyl platinum(II) acetylides. *Coord. Chem. Rev.* **2006**, *250* (13), 1819−1828. (b) Wong, W.-Y.; Ho, C.-L. Organometallic photovoltaics: A new and versatile approach for harvesting solar energy using conjugated polymetallaynes. *Acc. Chem. Res.* **2010**, *43* (9), 1246−1256. (c) Chan, A. K.-W.; Yam, V. W.-W. Precise modulation of molecular building blocks from tweezers to rectangles for recognition and stimuli-responsive processes. *Acc. Chem. Res.* **2018**, *51* (12), 3041−3051. (d) Cardolaccia, T.; Li, Y.; Schanze, K. S. Phosphorescent platinum acetylide organogelators. *J. Am. Chem. Soc.* **2008**, *130* (8), 2535−2545.

(30) (a) Yuen, M.-Y.; Roy, V. A. L.; Lu, W.; Kui, S. C. F.; Tong, G. S. M.; So, M.-H.; Chui, S. S.-Y.; Muccini, M.; Ning, J. Q.; Xu, S. J.; Che, C.-M. Semiconducting and electroluminescent nanowires self-assembled from organoplatinum(II) complexes. *Angew. Chem., Int. Ed.*

https://dx.doi.org/10.1021/jacs.0c06680
J. Am. Chem. Soc. XXXX, XXX, XXX−XXX

2008, *47* (51), 9895−9899. (b) Strassert, C. A.; Chien, C.-H.; Galvez Lopez, M. D.; Kourkoulos, D.; Hertel, D.; Meerholz, K.; De Cola, L. Switching on luminescence by the self-assembly of a platinum(II) complex into gelating nanofibers and electroluminescent films. *Angew. Chem., Int. Ed.* **2011**, *50* (4), 946−950. (c) Leung, S. Y. L.; Wong, K. M. C.; Yam, V. W. W. Self-assembly of alkynylplatinum(II) terpyridine amphiphiles into nanostructures via steric control and metal-metal interactions. *Proc. Natl. Acad. Sci. U. S. A.* **2016**, *113* (11), 2845−2850. (d) Li, Y. G.; Chen, L.; Ai, Y. Y.; Hong, E. Y. H.; Chan, A. K. W.; Yam, V. W. W. Supramolecular self-assembly and dual-switch vapochromic, vapoluminescent, and resistive memory behaviors of amphiphilic platinum(II) complexes. *J. Am. Chem. Soc.* **2017**, *139* (39), 13858−13866. (e) Chan, M. H. Y.; Leung, S. Y. L.; Yam, V. W. W. Controlling self-assembly mechanisms through rational molecular design in oligo(p-phenyleneethynylene)-containing alkynylplatinum(II) 2,6-bis(n-alkylbenzimidazol-2 '-yl)pyridine amphiphiles. *J. Am. Chem. Soc.* **2018**, *140* (24), 7637−7646. (f) Lu, W.; Chen, Y.; Roy, V. A. L.; Chui, S. S.-Y.; Che, C.-M. Supramolecular polymers and chromonic mesophases self-organized from phosphorescent cationic organoplatinum(II) complexes in water. *Angew. Chem., Int. Ed.* **2009**, *48* (41), 7621−7625. (g) Yu-Lut Leung, S.; Wing-Wah Yam, V. Hierarchical helices of helices directed by Pt Pt and π-π stacking interactions: reciprocal association of multiple helices of dinuclear alkynylplatinum(II) complex with luminescence enhancement behavior. *Chem. Sci.* **2013**, *4* (11), 4228−4234.

(31) (a) Ravotto, L.; Ceroni, P. Aggregation induced phosphorescence of metal complexes: From principles to applications. *Coord. Chem. Rev.* **2017**, *346*, 62−76. (b) You, Y.; Huh, H. S.; Kim, K. S.; Lee, S. W.; Kim, D.; Park, S. Y. Comment on 'aggregation-induced phosphorescent emission (AIPE) of iridium(III) complexes': origin of the enhanced phosphorescence. *Chem. Commun.* **2008**, No. 34, 3998−4000. (c) Zhao, Q.; Li, L.; Li, F.; Yu, M.; Liu, Z.; Yi, T.; Huang, C. Aggregation-induced phosphorescent emission (AIPE) of iridium(III) complexes. *Chem. Commun.* **2008**, No. 6, 685−687. (d) Liu, S.; Sun, H.; Ma, Y.; Ye, S.; Liu, X.; Zhou, X.; Mou, X.; Wang, L.; Zhao, Q.; Huang, W. Rational design of metallophosphors with tunable aggregation-induced phosphorescent emission and their promising applications in time-resolved luminescence assay and targeted luminescence imaging of cancer cells. *J. Mater. Chem.* **2012**, *22* (41), 22167−22173.

(32) Fu, H. L. K.; Po, C.; Leung, S. Y. L.; Yam, V. W. W. Self-assembled architectures of alkynylplatinum(II) amphiphiles and their structural optimization: a balance of the interplay among Pt···Pt, pi-pi stacking, and hydrophobic-hydrophobic interactions. *ACS Appl. Mater. Interfaces* **2017**, *9* (3), 2786−2795.

(33) Chan, Y.-T.; Li, X.; Soler, M.; Wang, J.-L.; Wesdemiotis, C.; Newkome, G. R. Self-assembly and traveling wave ion mobility mass spectrometry analysis of hexacadmium macrocycles. *J. Am. Chem. Soc.* **2009**, *131* (45), 16395−16397.

(34) (a) Wang, H.; Li, Y.; Yu, H.; Song, B.; Lu, S.; Hao, X.-Q.; Zhang, Y.; Wang, M.; Hla, S.-W.; Li, X. Combining synthesis and self-assembly in one pot to construct complex 2D metallo-supramolecules using terpyridine and pyrylium salts. *J. Am. Chem. Soc.* **2019**, *141* (33), 13187−13195. (b) Li, Z.; Li, Y.; Zhao, Y.; Wang, H.; Zhang, Y.; Song, B.; Li, X.; Lu, S.; Hao, X.-Q.; Hla, S.-W.; Tu, Y.; Li, X. Synthesis of metallopolymers and direct visualization of the single polymer chain. *J. Am. Chem. Soc.* **2020**, *142* (13), 6196−6205.

(35) Kong, F. K. W.; Tang, M. C.; Wong, Y. C.; Ng, M.; Chan, M. Y.; Yam, V. W. W. Strategy for the realization of efficient solution-processable phosphorescent organic light-emitting devices: Design and synthesis of bipolar alkynylplatinum(II) complexes. *J. Am. Chem. Soc.* **2017**, *139* (18), 6351−6362.

(36) (a) Wang, K.; Haga, M.-a.; Monjushiro, H.; Akiba, M.; Sasaki, Y. Luminescent langmuir-blodgett films of platinum(II) complex [Pt(L18)Cl](PF_6) (L18 = 2,6-bis(1-octadecylbenzimidazol-2-yl)-pyridine). *Inorg. Chem.* **2000**, *39* (18), 4022−4028. (b) Mathew, I.; Sun, W. Photophysics in solution and Langmuir-Blodgett film and vapochromic behavior of the Pt(II) 2,6-bis(N-alkylbenzimidazol-2'-yl)pyridine complexes with different alkyl chains and counter anions. *Dalton Trans.* **2010**, *39* (25), 5885−5898.

(37) (a) Ji, Z.; Azenkeng, A.; Hoffmann, M.; Sun, W. Synthesis and photophysics of 4'-R-2,2';6',2″-terpyridyl (R = Cl, CN, $N(CH_3)_2$) platinum(II) phenylacetylide complexes. *Dalton Trans.* **2009**, No. 37, 7725−7733. (b) Shao, P.; Li, Y.; Yi, J.; Pritchett, T. M.; Sun, W. Cyclometalated platinum(II) 6-phenyl-4-(9,9-dihexylfluoren-2-yl)-2,2'-bipyridine complexes: synthesis, photophysics, and nonlinear absorption. *Inorg. Chem.* **2010**, *49* (10), 4507−4517.

(38) Po, C.; Wing-Wah Yam, V. A metallo-amphiphile with unusual memory behaviour: effect of temperature and structure on the self-assembly of triethylene glycol (TEG)-pendant platinum(II) bzimpy complexes. *Chem. Sci.* **2014**, *5* (12), 4868−4872.

(39) Au-Yeung, H. L.; Tam, A. Y. Y.; Leung, S. Y. L.; Yam, V. W. W. Supramolecular assembly of platinum-containing polyhedral oligomeric silsesquioxanes: an interplay of intermolecular interactions and a correlation between structural modifications and morphological transformations. *Chem. Sci.* **2017**, *8* (3), 2267−2276.

(40) (a) Czerwiski, A.; Sobkowski, J. Kinetics of adsorbed "CO_2" oxidation on a platinum electrode. *J. Electroanal. Chem. Interfacial Electrochem.* **1975**, *59* (1), 41−46. (b) Ishiji, T.; Takahashi, K.; Kira, A. Amperometric carbon dioxide gas sensor based on electrode reduction of platinum oxide. *Anal. Chem.* **1993**, *65* (65), 2736−2739. (c) Wang, H.; Zhang, L.; Zhou, Y.; Qiao, S.; Liu, X.; Wang, W. Photocatalytic CO_2 reduction over platinum modified hexagonal tungsten oxide: Effects of platinum on forward and back reactions. *Appl. Catal., B* **2020**, *263*, 118331.

(41) (a) Yuan, H.; Tao, J.; Li, N.; Karmakar, A.; Tang, C.; Cai, H.; Pennycook, S. J.; Singh, N.; Zhao, D. On-chip tailorability of capacitive gas sensors integrated with metal-organic framework films. *Angew. Chem., Int. Ed.* **2019**, *58* (40), 14089−14094. (b) Yuan, H.; Li, N.; Linghu, J.; Dong, J.; Wang, Y.; Karmakar, A.; Yuan, J.; Li, M.; Buenconsejo, P. J. S.; Liu, G.; Cai, H.; Pennycook, S. J.; Singh, N.; Zhao, D. Chip-level integration of covalent organic frameworks for rrace benzene sensing. *ACS Sensors* **2020**, *5* (5), 1474−1481.

(42) (a) Che, C.-M.; Chow, C.-F.; Yuen, M.-Y.; Roy, V. A. L.; Lu, W.; Chen, Y.; Chui, S. S.-Y.; Zhu, N. Single microcrystals of organoplatinum(II) complexes with high charge-carrier mobility. *Chem. Sci.* **2011**, *2* (2), 216−220. (b) Kong, F. K. W.; Chan, A. K. W.; Ng, M.; Low, K. H.; Yam, V. W. W. Construction of discrete pentanuclear platinum(II) stacks with extended metal-metal interactions by using phosphorescent platinum(II) tweezers. *Angew. Chem., Int. Ed.* **2017**, *56* (47), 15103−15107.

https://dx.doi.org/10.1021/jacs.0c06680
J. Am. Chem. Soc. XXXX, XXX, XXX−XXX